Journal of Catalysis **186,** 242–253 (1999)
Article ID jcat.1999.2548, available online at http://www.idealibrary.com on IDEAL®

Investigations of the State of Fe in H–ZSM-5

Lisa J. Lobree, In-Chul Hwang, Jeffrey A. Reimer, and Alexis T. Bell

Chemical Sciences Division, Lawrence Berkeley National Laboratory, and Department of Chemical Engineering, University of California, Berkeley, California 94720

Received October 7, 1998; revised May 6, 1999; accepted May 7, 1999

The state of Fe dispersion in Fe–H–ZSM-5 was investigated by means of infrared spectroscopy of adsorbed NO, temperature-programmed desorption (TPD) of NO, TPD of NH_3, and H_2 temperature-programmed reduction (TPR). For samples with a low loading of Fe [e.g., Fe/Al ratio $\leq$ 0.56], Fe cations exchange with Brønsted acid protons on a one-to-one basis, while at Fe/Al ratios above this level small particles of FeO_x are formed. Results of H_2 TPR and NO uptake experiments on Fe–ZSM-5 samples following a He pretreatment suggest that the primary form of Fe present on samples with an Fe/Al ratio less than or equal to 0.19 is Fe^{3+} [i.e., $Fe^{3+}(OH^-)_2$]. An increase in the Fe loading above this level results in an increase in the concentration of Fe^{2+} cations formed via the autoreduction of $Fe^{3+}(OH^-)_2$ which is present at highly reducible α sites in ZSM-5. Three types of Fe^{2+} sites are observed on Fe–ZSM-5 during the room temperature adsorption of NO. They are defined as type I, II, and III sites. Type I sites adsorb NO as mononitrosyls (1767 cm^{-1}) and dinitrosyls (1917 and 1806 cm^{-1}). Types II and III sites adsorb NO solely as mononitrosyl species (1876 and 1856 cm^{-1}, respectively). While types II and III sites are found to be relatively resistant to oxidation and reduction, type I sites are significantly affected by these pretreatments. The most notable change occurs for the high-weight-loaded Fe–ZSM-5 sample in which CO reduction results in the redispersion of FeO_x to type I sites. © 1999 Academic Press

INTRODUCTION

The performance of metal-exchanged ZSM-5 catalysts for the reduction of NO by hydrocarbons in the presence of excess O_2 is generally inhibited by the presence of water. It has been determined recently, however, that Fe exchanged into ZSM-5 is active for NO reduction by isobutane in the presence of H_2O vapor at concentrations as high as 20% (1–4). The preparation of Fe–ZSM-5 with a high loading of iron has proven to be a challenge. While Feng and Hall (1, 2) reported that an Fe/Al ratio up to 0.93 could be achieved by ion exchange of Na–ZSM-5 using a saturated aqueous solution of ferrous oxalate (1, 2), attempts by Chen and Sachtler (3, 4) to use this procedure were unsuccessful in achieving such high exchange levels. Moreover, these latter authors noted that differences in catalyst performance were observed which appeared to be related to subtle differences in zeolite history. Reproducible performance could be achieved, though, using dry exchange of H–ZSM-5 with $FeCl_3$. In a related study, ion exchange with $Fe(NO_3)_3$ was carried out with ZSM-5 (5).

Only limited characterization of Fe–ZSM-5 has been reported to date. Microbalance analysis of samples following O_2/H_2 redox cycles has shown that a reversible oxidation–reduction process occurs with a redox couple equivalent to 1 electron/Fe for catalysts treated at or below 1223 K, suggesting a cycle between Fe^{2+} and Fe^{3+} (2). When the same experiment was performed at 1323 K, the results showed a redox couple of approximately 2 electrons/Fe. Evidence for the positioning of Fe cations in the ion-exchange position has been obtained from both ^1H NMR (2) and infrared spectroscopy (3). In both cases, no evidence for Brønsted acid protons was observed after exchange to an Fe/Al ratio approaching unity. Evidence for nanoclusters of iron oxide obtained by EXAFS has been reported, though, for Fe–ZSM-5 prepared by aqueous ion exchange from ferric nitrate (5).

The preceding work suggests that different forms of iron can exist in Fe–ZSM-5 and that iron is not present in a single oxidation state but can be oxidized and reduced. The goal of the present work was to determine the effects of Fe loading on the state of Fe in Fe–ZSM-5 prepared via solid state ion exchange. It was of particular interest to determine the degree to which Fe is present in cation-exchange positions versus iron oxide clusters, and the oxidation state of Fe cations following different forms of pretreatment. The samples of Fe–ZSM-5 were characterized by infrared spectroscopy of adsorbed NO, temperature-programmed desorption (TPD) of NO, TPD of NH_3, and H_2 temperature-programmed reduction (TPR).

EXPERIMENTAL

Fe–ZSM-5 was prepared via a solid state ion-exchange method similar to that described by Chen *et al.* (3, 4). Na–ZSM-5 (Si/Al = 25) obtained from Alsi-Penta was first converted to the NH_4^+ form by aqueous ion exchange with ammonium nitrate. About 10 g of the zeolite was added to a 120-ml solution of 1.0 M ammonium nitrate. This mixture

0021-9517/99 $30.00
Copyright © 1999 by Academic Press
All rights of reproduction in any form reserved.

TABLE 1

Sample Characteristics

Sample	wt% Fe	Fe/g (μmol/g)
Fe–ZSM-5 (0.14)	0.49	87.7
Fe–ZSM-5 (0.19)	0.67	120.0
Fe–ZSM-5 (0.37)	1.26	225.6
Fe–ZSM-5 (0.56)	1.94	347.4
Fe–ZSM-5 (0.85)	2.61	467.3
Fe–ZSM-5 (0.96)	2.86	512.1

was stirred at 298 K for 12 h, then filtered, and washed. To assure complete displacement of Na^+ by NH_4^+, the exchange procedure was repeated two more times. NH_4^+–ZSM-5 was then transformed to H–ZSM-5 by calcining at 823 K for 8 h in air. The calcined H–ZSM-5 was then transferred to a glove box without contacting air and mechanically mixed with the appropriate amount of $FeCl_3$ required for the desired exchange level. While still in the glove box, this mixture was placed into a sealed reactor. The reactor was then removed from the glove box and placed in a furnace. A flow of He was passed through the reactor as it was heated at a rate of 0.25 K/min to 583 K, the sublimation temperature of $FeCl_3$. Upon the temperature reaching 583 K, the reactor was held at this temperature for 4 h. The sample was then cooled to room temperature, removed from the reactor, and washed with water until the precipitation of AgCl was not detected upon the addition of $AgNO_3$ to the residual water. Finally, the Fe–ZSM-5 was dried in an oven overnight at 393 K. Elemental analysis was performed on all samples and the results are shown in Table 1. The samples are denoted as Fe–ZSM-5 (x) where x is the Fe/Al ratio. All samples exhibited a residual Na/Al ratio of less than 0.05. The properties of Fe–ZSM-5 were compared with those of silica-supported Fe and bulk Fe_2O_3. Then, 3.3 wt% Fe/SiO_2 was prepared by incipient wetness impregnation using an aqueous solution of $Fe(NO_3)_3 \cdot 9H_2O$ with a liquid/solid ratio of 2.2 cm^3/g followed by calcination at 773 K for 3 h in air. Bulk Fe_2O_3 (Matheson, Coleman and Bell) was used as is.

Temperature-programmed desorption of NH_3 was performed to determine the residual acidity in the Fe–ZSM-5 samples. Prior to use, the samples were heated at 773 K for 1 h in He and then cooled to room temperature in He. NH_3 was adsorbed for 1 h at room temperature on 0.1 g of sample sieved to 35–60 mesh from a gas stream containing 2% NH_3 in He (Airgas). Following adsorption, the sample was purged in He for 1 h, and then a temperature ramp of 10 K/min was initiated from room temperature to 873 K. The concentration of NH_3 in the effluent was detected by a thermal conductivity detector.

Temperature-programmed reduction in H_2 was performed using the same system as that described for the temperature-programmed desorption of NH_3. Then, 1% H_2 in Ar (Matheson) was passed over the sample at room temperature for 10 min prior to initiating a temperature ramp of 10 K/min. Water formed during the reduction of Fe was removed by a dry ice–methanol trap located downstream of the reactor and ahead of the TCD. The response of the TCD to flowing H_2 was calibrated by performing a temperature-programmed reduction of a known amount of CuO.

NO uptake was determined by performing temperature-programmed desorption of NO and quantifying the total amount of NO adsorbed by summing the nitrogen products. Experiments were carried out with 0.1 g of catalyst sieved to 35–60 mesh and placed in a quartz microreactor. The NO (Matheson, 1% in He) was further purified by passage through a molecular sieve trap to remove residual water. The NO was diluted to 5,000 ppm NO in He and was then adsorbed on the zeolite at room temperature. The sample was purged with He for 1 h to remove weakly adsorbed NO, and then a temperature ramp of 8 K/min was initiated. NO was desorbed into He flowing at 100 cm^3/min; desorbing species were monitored via mass spectrometry (UTI 100 C).

For infrared spectroscopy of adsorbed NO, the Fe–ZSM-5 was pressed into a 20- to 50-mg self-supporting wafer and placed into an infrared cell similar to that described by Joly *et al.* (6). Spectra were recorded on a Digilab FTS-50 Fourier transform infrared spectrometer at a resolution of 4 cm^{-1}. Typically, 64 scans were co-added to obtain a good signal-to-noise ratio. A reference spectrum of Fe–ZSM-5 in He, taken at the same temperature as the experimental spectrum, was subtracted from each spectrum. NO (Matheson, 5% in He) was passed through a molecular sieve trap for additional purification prior to entering the flow manifold. Prior to adsorption on the zeolite, the NO was diluted to a concentration of 5,000 ppm.

A separate cell and spectrometer were used to observe the hydroxyl stretching region of the zeolites. For these experiments, spectra were recorded using a Nicolet Magna Series II Fourier transform infrared spectrometer. The cell design for this spectrometer limits the maximum sample temperature to 523 K; hence, the sample had to be pretreated *ex situ* in a separate reactor. Prior to each experiment, the sample was heated at 773 K in He for 1 h and then cooled to room temperature. The sample was then removed from the reactor and pressed into a 20- to 30-mg wafer that was then put into the infrared cell. To remove water adsorbed during sample transfer, the zeolites were treated by heating the sample in He for 1 h at 523 K and then cooling to 323 K prior to obtaining the spectrum. Each spectrum was obtained from 256 scans taken at a resolution of 4 cm^{-1} and was normalized by sample weight.

Unless otherwise specified, prior to each experiment, the catalyst was given one of the following pretreatments: (1) helium (H), heat at 773 K for 3 h in He and cool to room temperature in He; (2) oxidative (O), heat at 773 K in 10% O_2 for 2 h, heat at 773 K in He for 1 h, and cool to room

TABLE 2

Description of Catalyst Pretreatments (Steps (1) and (2) Performed at 773 K)

Symbol	Pretreatment	Step (1)	Step (2)	Step (3)
H	Helium	He, 2 h	He, 1 h	cool in He
O	Oxidative	10% O_2, 2 h	He, 1 h	cool in He
R	Reductive	4.2% CO, 2 h	He, 1 h	cool in He

temperature in He; and (3) reductive (R), heat at 773 K in 4.2% CO for 2 h, heat at 773 K in He for 1 h, and cool to room temperature in He. Table 2 summarizes each sample pretreatment protocol. Note that for the experiments involving the uptake of NO and infrared spectroscopy of adsorbed NO these pretreatments were conducted consecutively on the same sample, while a fresh sample was used for each H_2 TPR experiment.

RESULTS

The temperature-programmed desorption of NH_3 following room-temperature adsorption from a stream containing 2% NH_3 in He is shown in Fig. 1. As noted previously, the samples were pretreated in He prior to conducting the NH_3 TPD. NH_3 desorbs in three main peaks at 383, 473, and 703 K. The peak at 383 K is assigned to physisorbed NH_3 while the peak at 703 K is assigned to NH_3 strongly adsorbed on Brønsted acid sites (7). Assignment of the peak at 473 K is somewhat controversial. This feature has been attributed to NH_3 weakly adsorbed on Brønsted acid sites (7) and NH_3 associated with Na^+ (8) or extraframework Al (9). Since it is agreed that the peak at 703 K is due only to NH_3 strongly adsorbed on Brønsted acid sites, this peak can be used to observe qualitative changes in the concentration of Brønsted acid sites with Fe loading. The data in Fig. 1 show that the peak at 703 K decreases with increasing Fe content, suggesting that Brønsted acid protons are replaced by Fe upon heating H–ZSM-5 in the presence of $FeCl_3$. The intensity of the peak at 473 K also decreases with increasing Fe content, supporting the attribution of this peak to weak Brønsted acid sites. Note that an increasing Fe content results in a nonzero background level at 873 K.

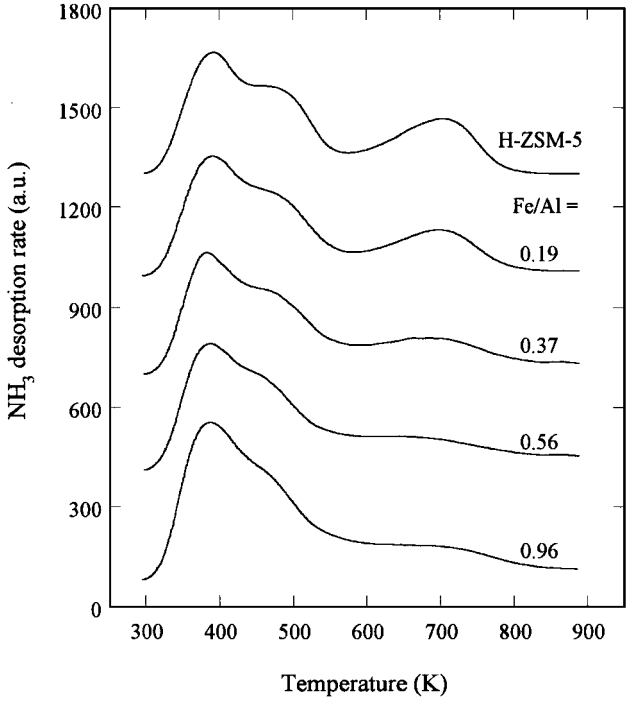

FIG. 1. NH_3 desorption rate observed during the temperature-programmed desorption of NH_3 into He following room-temperature exposure of Fe–ZSM-5 samples to 2% NH_3 in He for 1 h.

Infrared spectra of the samples were taken at 323 K in He to measure the concentration of Brønsted acid sites remaining following ion exchange. The results are shown in Fig. 2. Bands are observed at 3740, 3660, and 3610 cm^{-1}. The band at 3740 cm^{-1} has been assigned to hydroxyl stretching at Si(OH) groups at crystal terminations and silanol pairs (10) while the band at 3660 cm^{-1} has been assigned to OH groups associated with extraframework Al (11, 12). The band at 3610 cm^{-1} is due to the OH stretch of Brønsted acid groups (13). There is also a band present at 3700 cm^{-1} on H–ZSM-5; however, this band was not present on an H–ZSM-5 sample with a lower Si/Al ratio, and it is not clear why it is observed on this sample. The principal effect of increased Fe exchange is a decrease in the intensity of the band at 3610 cm^{-1}, giving direct evidence for the displacement of Brønsted acid protons by Fe. While the band at 3660 cm^{-1} is unaffected by Fe loading, the band at 3740 cm^{-1} changes with Fe content. There is no identifiable trend in this data and it is likely that this apparent change is associated with a change in the overall absorption of the background which was a function of Fe loading and hence sample color.

The number of Fe atoms replacing each Brønsted proton can be determined by integrating the area of the band at 3610 cm^{-1} and plotting the H/Al ratio versus the Fe/Al ratio. The concentration of Brønsted acid sites in the Fe–ZSM-5 samples (H/Al ratio) was calculated by normalizing the integrated area of the band at 3610 cm^{-1} to the area observed for H–ZSM-5. The results are shown in Fig. 3. If one Fe replaces one proton, then the data in Fig. 3 should fall along a line with a slope of −1, whereas replacement of two protons with one Fe should result in a line with a slope of −2. Up to an Fe/Al ratio of 0.56, the data lie along a line with slope −1, suggesting a 1 : 1 exchange of Brønsted acid protons and Fe ions. However, above this Fe loading, the data deviate upward, suggesting that the additional Fe is present as FeO_x particles rather than as Fe^{n+} cations replacing H^+.

Figure 4 shows the temperature-programmed reduction profiles for Fe_2O_3 and 3.3 wt% Fe/SiO_2. The 3.3 wt%

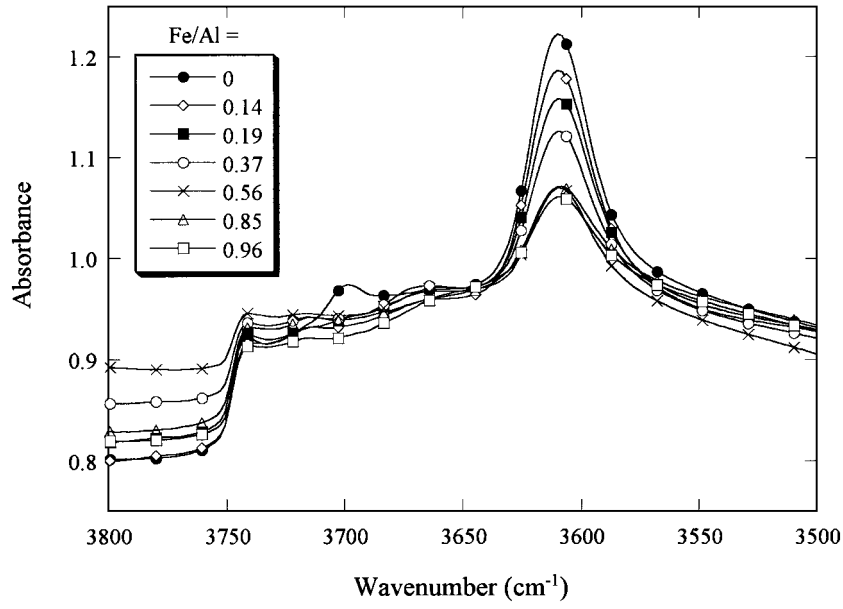

FIG. 2. Infrared spectra of the hydroxyl stretching region for Fe–ZSM-5 samples at 323 K following a helium pretreatment.

Fe/SiO_2 sample was heated in O_2 at 773 K for 2 h, followed by a 1-h He purge prior to conducting TPR and the Fe_2O_3 sample was used as is. The reduction of bulk Fe_2O_3 results in two main peaks at 693 and 963 K with a small shoulder at 863 K. The peak at 693 K is due to the reduction of Fe_2O_3 to Fe_3O_4, while the peak observed at 963 K is assigned to the reduction of Fe_3O_4 to Fe^0 (14). Since the reduction of Fe_3O_4 to Fe^0 proceeds via FeO, the small shoulder at 863 K is assigned to the reduction of Fe_3O_4 to FeO (14). Integration of the TPR data for Fe_2O_3 yields an H_2/Fe ratio of 1.54, consistent with the value of 1.50 required for the reduction of Fe^{3+} to Fe^0. TPR of Fe/SiO_2 results in a peak at 723 K, followed by the initiation of further reduction beginning at 1250 K. Integrating the low-temperature peak yields a H_2/Fe ratio of 0.52. This value agrees with the ratio of 0.50 necessary for the reduction of Fe^{3+} to Fe^{2+}. Consistent with this observation, it has been shown for Fe/SiO_2 that Fe^{2+} is present in small "rafts" of iron oxide which are very stable against reduction to metallic iron during H_2 reduction (15).

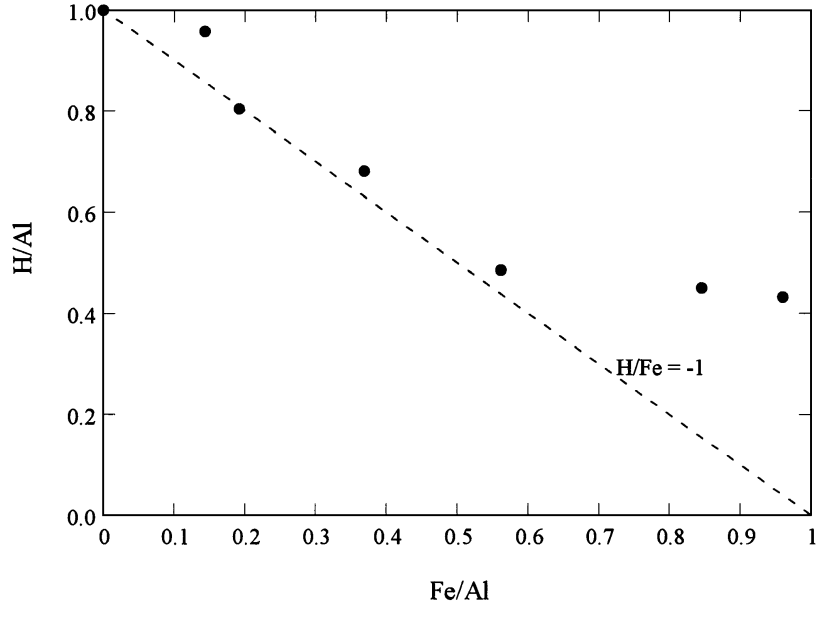

FIG. 3. Variation of the H/Al ratio with Fe/Al ratio for all Fe–ZSM-5 samples pretreated in helium.

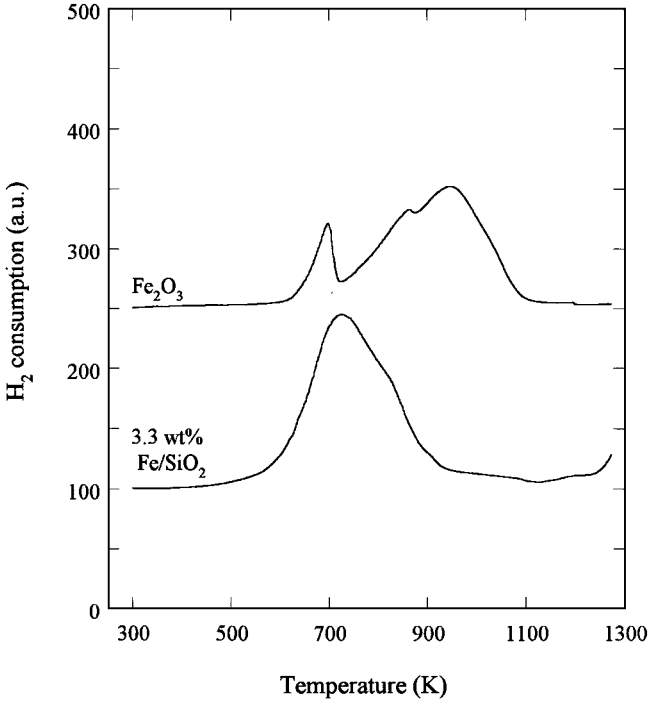

FIG. 4. H_2 temperature-programmed reduction profiles observed for Fe_2O_3 and 3.3 wt% Fe/SiO_2. The 3.3 wt% Fe/SiO_2 samples was given a standard pretreatment (O) while the Fe_2O_3 was used as is.

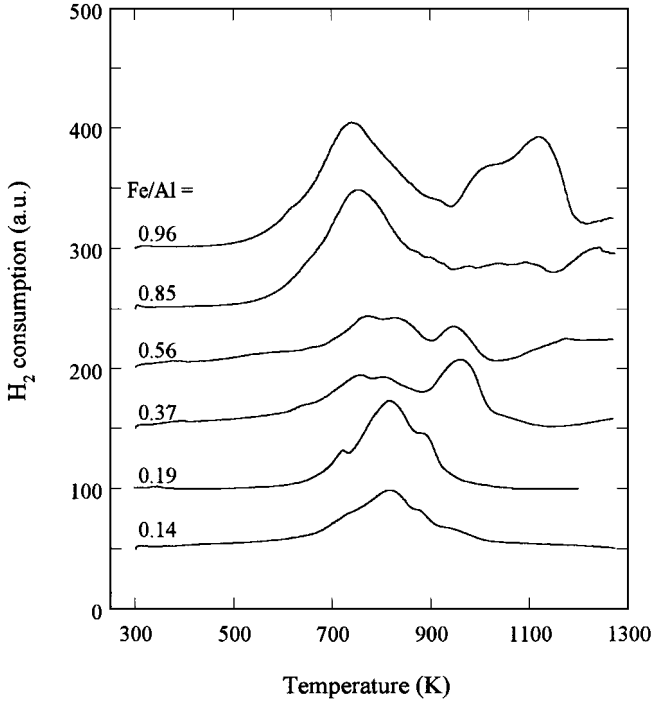

FIG. 5. H_2 temperature-programmed reduction profiles observed for all Fe-ZSM-5 samples following a helium pretreatment (H).

TPR experiments were conducted on all Fe–ZSM-5 samples following a He pretreatment (H). The results are shown in Fig. 5. The TPR spectrum for the sample with the smallest amount of Fe exchange [Fe–ZSM-5 (0.14)] exhibits one main peak at 815 K. The profile for Fe–ZSM-5 (0.19) is similar to that observed for Fe–ZSM-5 (0.14), except the two shoulders present at 720 and 890 K are more prominent. As the Fe content increases, the shape of the TPR profile changes. On Fe–ZSM-5 (0.37), the peak at 815 K becomes slightly smaller and a new peak emerges at 960 K. Further loading [Fe–ZSM-5 (0.56)] results in the same peaks at 815 and 960 K and a tail that is present to temperatures higher than 1273 K. Note that the integrated area of the peak at 815 K decreases slightly with an increase in Fe exchange for these samples. The samples with the highest loading of Fe [Fe–ZSM-5 (0.85 and 0.96)] differ significantly in character when compared to the other samples. The total integrated area is larger and new peaks are evident at 738 K for Fe–ZSM-5 (0.85 and 0.96) and 1015 and 1120 K for Fe–ZSM-5 (0.96).

Table 3 summarizes the H_2/Fe ratio determined by integration from room temperature to 1273 K for all samples following a He pretreatment (H) and an oxidative pretreatment (O) (see below). The extent of reduction is highest for Fe–ZSM-5 (0.14). In this case, the H_2/Fe ratio based on integration to 1273 K is 1.34, suggesting that a significant portion of Fe present as Fe^{3+} initially is reduced to Fe^0. The H_2/Fe ratio for Fe–ZSM-5 (0.19) is similar to that for Fe–ZSM-5 (0.14). As the Fe loading is increased [Fe–ZSM-5 (0.37 and 0.56)], the H_2/Fe ratio decreases to values less than 1. A further increase in the Fe loading [Fe–ZSM-5 (0.85 and 0.96)] results in an increase in the H_2/Fe ratio to a maximum value of 0.81; however, this value is still significantly smaller than that observed on Fe–ZSM-5 (0.14).

Figure 6 shows the results of temperature-programmed reduction experiments conducted following an oxidative pretreatment (O) on fresh samples of Fe–ZSM-5 and Table 3 lists the H_2/Fe consumption ratio for each sample. Comparison of the TPR spectra in Fig. 6 with those in Fig. 5 shows that oxidation causes an increase in the intensity of the peaks occurring in the region of 500–750 K and above 900 K. Note that with the exception of Fe–ZSM-5 (0.19)

TABLE 3

H_2/Fe Consumption Ratios Derived from TPR Spectra

Sample	Pretreatment H H_2/Fe	Pretreatment O H_2/Fe
Fe–ZSM-5-25 (0.14)	1.34	—
Fe–ZSM-5-25 (0.19)	1.33	1.36
Fe–ZSM-5-25 (0.37)	0.76	1.13
Fe–ZSM-5-25 (0.56)	0.52	0.82
Fe–ZSM-5-25 (0.85)	0.78	—
Fe–ZSM-5-25 (0.96)	0.81	0.99

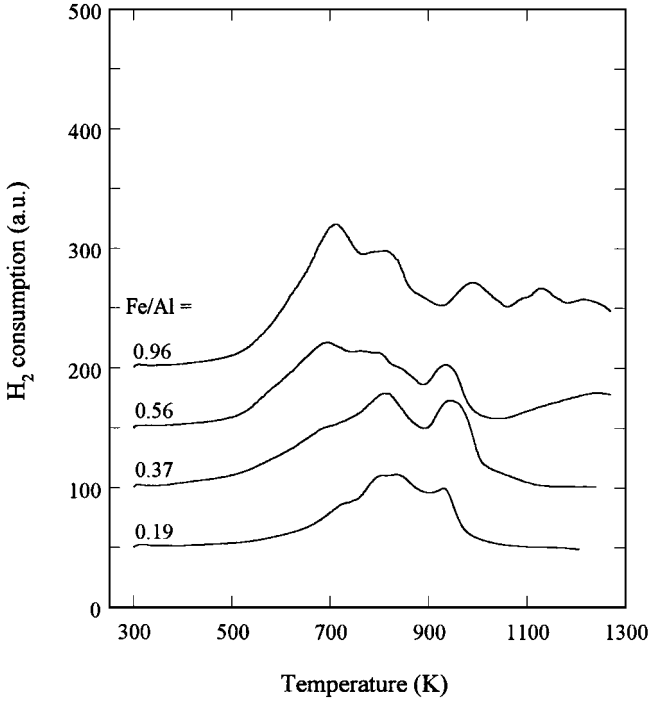

FIG. 6. H_2 temperature-programmed reduction profiles observed for Fe–ZSM-5 samples following an oxidative pretreatment (O).

oxidation results in an increase in the H_2/Fe consumption ratio, relative to what is observed after pretreatment in He. These results suggest that Fe in Fe–ZSM-5 (0.19) is present as Fe^{3+}, but that samples prepared with Fe/Al > 0.19 contain a mixture of Fe^{2+} and Fe^{3+}.

Figure 7 shows the temperature-programmed reduction of Fe–ZSM-5 (0.96) following pretreatments H, O, and R. For an easier comparison, the reduction profiles following pretreatments H and O are repeated in this figure. TPR of Fe–ZSM-5 (0.96) following CO reduction results in a significant decrease in the extent of reduction by H_2. Also, the character of the TPR profile changes. The low-temperature peak has essentially disappeared in the TPR following CO reduction and very little reduction occurs up to 1273 K. The H_2/Fe ratio for the TPR of Fe–ZSM-5 (0.96) following CO reduction is 0.63.

Temperature-programmed desorption of NO was conducted on several Fe–ZSM-5 samples following pretreatments H, O, and R. The total amount of NO adsorbed was calculated by integration of the TPD spectra for the desorption of the observed products, NO and N_2 (the maximum amount of N_2 observed was 12% of the total amount of adsorbed NO). A plot of the moles of NO adsorbed per gram of catalyst versus the Fe/Al ratio is presented in Fig. 8A. Note that if the data are extrapolated to $y = 0$ for all pretreatments, the x intercept is a nonzero positive number equivalent to approximately 100 μmol of Fe/g of catalyst. This suggests that there is some fraction of Fe that does not adsorb NO and it is likely that this Fe is present as Fe^{3+}, since it has been observed that Fe^{3+} cations and Fe_2O_3 adsorb only a small amount of NO relative to Fe^{2+} cations (15, 16).

Figure 8B presents the same data as those shown in Fig. 8A, but is plotted as mole of NO adsorbed per mole of Fe as a function of Fe content. The NO/Fe ratio is 0.40 for Fe–ZSM-5 (0.19) following pretreatment H. As the content of Fe in the zeolite increases, the NO/Fe ratio increases and reaches a maximum of 0.96 for Fe–ZSM-5 (0.56) and then drops back down to 0.52 moles of NO/mole of Fe for Fe–ZSM-5 (0.96). Oxidation (O) has little affect on the NO/Fe ratio for Fe–ZSM-5 (0.19), while Fe–ZSM-5 (0.37, 0.56, and 0.96) exhibit a decrease in the NO/Fe ratio relative to pretreatment H. Note also that the NO/Fe ratio on Fe–ZSM-5 (0.19) is not significantly affected by CO reduction. However, with the exception of Fe–ZSM-5 (0.56), which has a slightly lower NO/Fe ratio when compared to that with pretreatment H, the Fe–ZSM-5 samples with the higher weight loading show an increase in the NO/Fe ratio relative to those with pretreatments H and O. Relative to that with pretreatment H, the most significant change in NO/Fe ratio is observed for Fe–ZSM-5 (0.96) and the final NO/Fe ratio is approximately constant for Fe–ZSM-5 (0.37, 0.56, and 0.96).

Figure 9A shows infrared spectra of several samples taken at room temperature in He following a 20-min

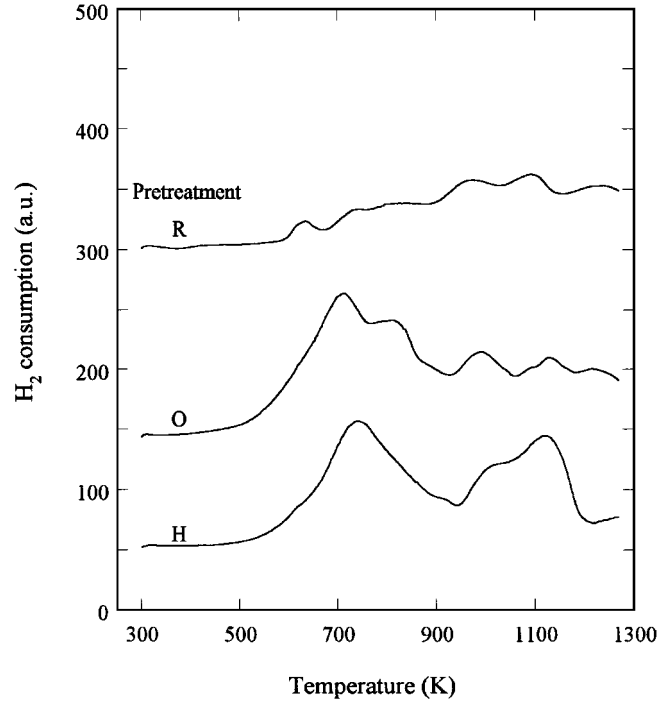

FIG. 7. H_2 temperature-programmed reduction profiles observed for Fe–ZSM-5 (0.96) following a helium (H), oxidative (O) and reductive (R) pretreatment.

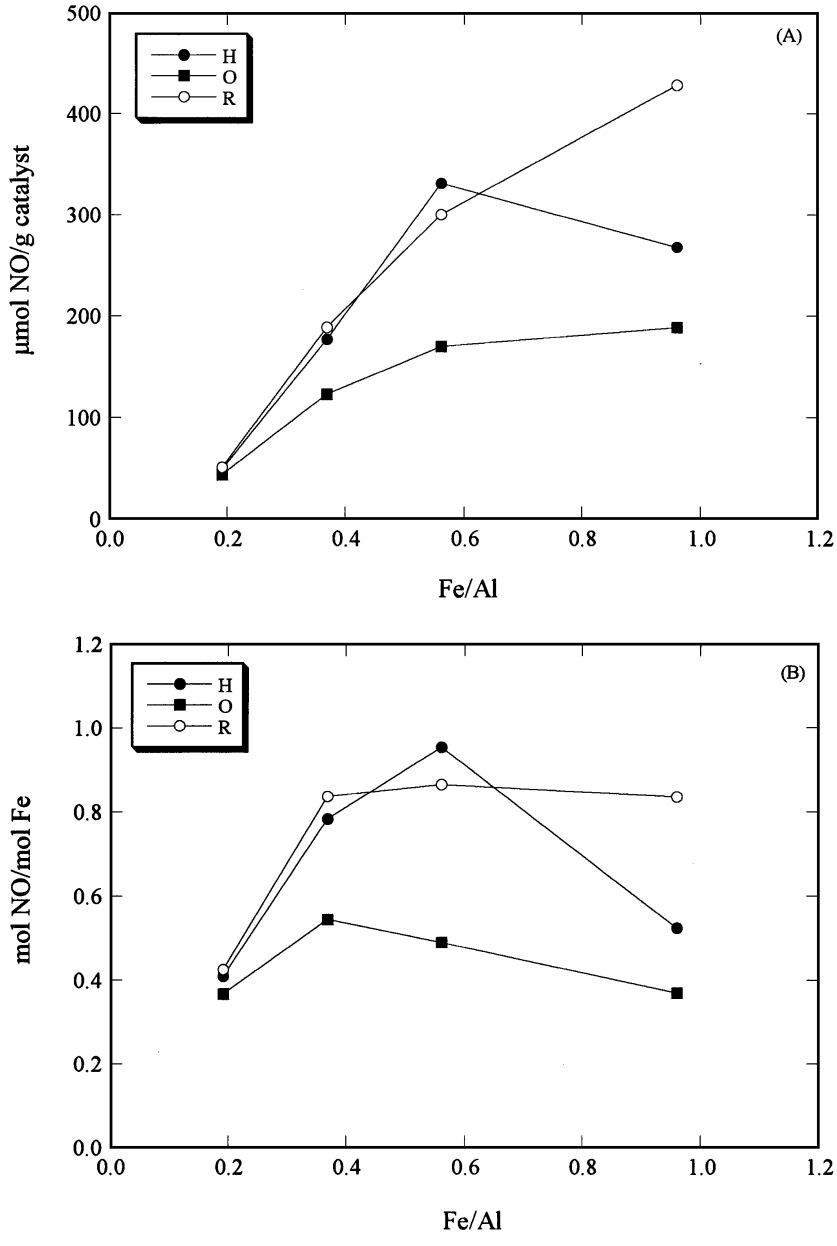

FIG. 8. (A) NO uptake per gram of catalyst as determined from NO temperature-programmed desorption for Fe–ZSM-5 samples following a helium (H), oxidative (O), and reductive (R) pretreatment. (B) NO uptake per Fe atom as determined from NO temperature-programmed desorption for Fe–ZSM-5 samples following a helium (H), oxidative (O), and reductive (R) pretreatment.

exposure to 5,000 ppm NO for samples pretreated in He. NO adsorption at room temperature results in four bands at 2133, 1876, 1856, and 1806 cm^{-1} with small shoulders at 1917 and 1767 cm^{-1}. While the bands at 1876 and 1856 cm^{-1} do not change with time, the intensity of the bands at 2133, 1917, 1806, and 1767 cm^{-1} increase slowly with time. On the basis of previous studies conducted with Fe–Y and Fe–ZMS-5 (17, 18), the pair of bands at 1917 and 1806 cm^{-1} are assigned to $Fe^{2+}(NO)_2$. The attribution of these bands to the same adsorbed species was confirmed by observing a straight line when the intensity of the band at 1917 cm^{-1} is plotted versus that at 1806 cm^{-1}. The band at 1767 cm^{-1} is assigned to an Fe^{2+} mononitrosyl [$Fe^{2+}(NO)$] that is in the same environment as the Fe^{2+} dinitrosyl (17, 18). The bands at 1876 and 1856 cm^{-1} are also due to Fe^{2+} mononitrosyls; however, these mononitrosyls exist in an environment different from the mononitrosyl characterized by the band at 1767 cm^{-1} (17, 18). The assignment of the band at 2133 cm^{-1} has been the subject of some discussion in the recent literature (19–22). Most investigators have attributed this band to NO_2^+ (22) or $NO_2^{\delta+}$ (19, 20); however, strong evidence has been presented recently (23) for the assignment of this

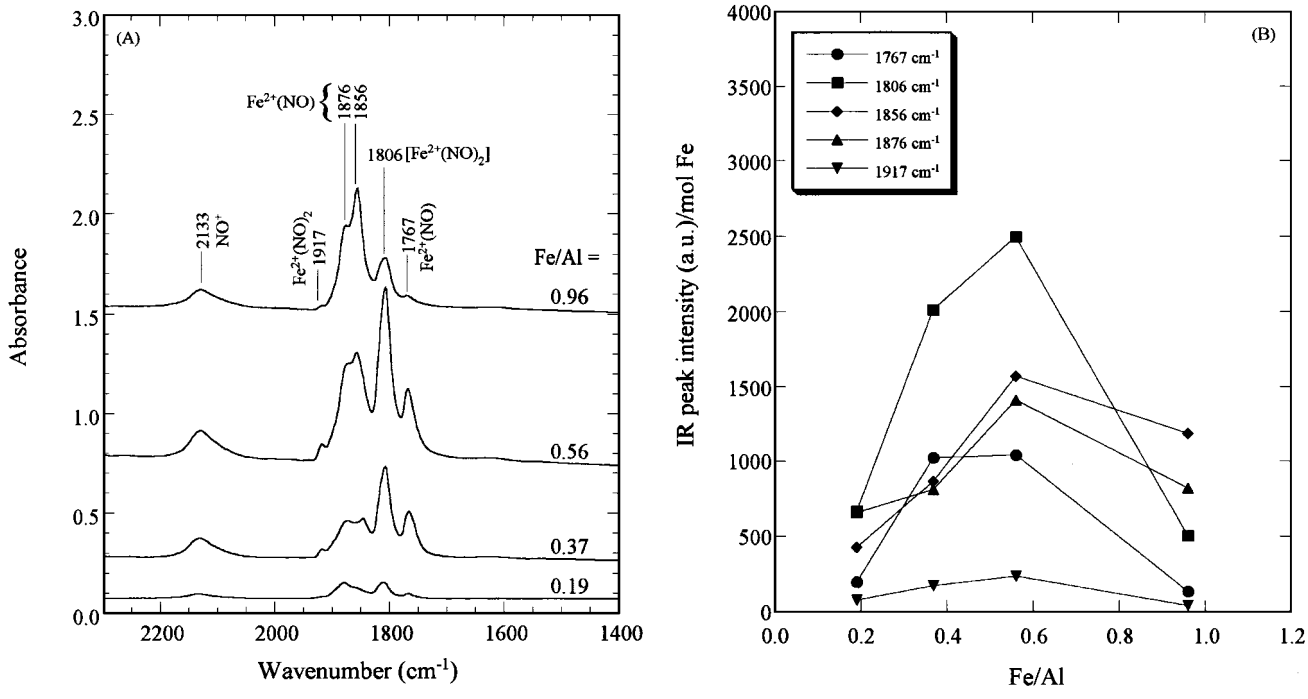

FIG. 9. (A) Infrared spectra of adsorbed NO for Fe–ZSM-5 samples following a helium pretreatment (H). (B) Intensity of infrared bands observed during the room-temperature adsorption of NO following a He pretreatment (H) versus Fe content.

band to NO^+, acting as the charge-compensating species at a cation-exchange site (e.g., Z^-NO^+). During the He purge, the bands at 2133, 1917, and 1806 cm^{-1} decrease slightly, while the band at 1767 cm^{-1} is observed to increase.

Figure 9B shows the intensity of the infrared bands due to NO adsorbed on Fe as a function of Fe content. For these samples an increase in the weight loading of Fe [Fe–ZSM-5 (0.19, 0.37 and 0.56)] results in an increase in the intensity of the bands. A further increase in the Fe content [Fe–ZSM-5 (0.96)] results in a significant decrease in the bands at 1917, 1806, and 1767 cm^{-1} while the bands at 1876 and 1856 cm^{-1} decrease only slightly.

Figures 10A and 10B show the infrared spectra and the peak intensities for samples following an oxidative pretreatment (O). While all bands are attenuated relative to the He–pretreated samples, the bands at 1917, 1806, and 1767 cm^{-1} exhibit the largest loss in intensity.

The infrared spectra for samples following CO reduction (R) are shown in Fig. 11A, and Fig. 11B shows the dependence of the band intensities on Fe loading. The intensity of the bands at 1876 and 1856 cm^{-1} is approximately the same as that observed following a He pretreatment. For Fe–ZSM-5 (0.19, 0.37, and 0.56) the intensity of the bands at 1917, 1806, and 1767 cm^{-1} is not significantly enhanced relative to He pretreatment, while the intensity of these bands for Fe–ZSM-5 (0.96) is much higher following a CO reduction as compared to He pretreatment. In light of this, the significant increase in NO uptake capacity for this sample following CO reduction (see Figs. 8A and 8B) can be associated with the adsorption of NO in the form of mono- and dinitrosyls.

DISCUSSION

The present study demonstrates that the state of dispersion and oxidation of Fe exchanged into H–ZSM-5 is a function of the Fe content and pretreatment. NH_3-TPD experiments performed on freshly prepared samples of Fe–ZSM-5 following He pretreatment show that the concentration of Brønsted acid sites decreases with an increase in Fe loading, suggesting that an iron chloride species replaces the Brønsted acid proton and acts as a charge-compensating ion. Consistent with this data, infrared experiments performed on Fe–ZSM-5 following a He pretreatment also show that Fe substitutes for Brønsted acid sites in H–ZSM-5. For samples with Fe/Al $\leq$ 0.56, iron is present as dispersed cations and substitutes for Brønsted acid protons on a 1 : 1 basis. However, the data shown in Fig. 3 suggest that at high Fe loadings [Fe–ZSM-5 (0.85 and 0.96)] a part of the Fe is present as FeO_x. The TPR spectrum observed for Fe–ZSM-5 (0.96) is qualitatively similar to that for Fe_2O_3, but the positions of the two principal peaks are different. The location of the low-temperature peak at 738 K is much closer to the peak observed for Fe/SiO_2 at 723 K, and the high-temperature peak occurs at 1000 K. The similarity of the low-temperature peak to that observed for Fe/SiO_2 suggests the presence of small particles of Fe_2O_3, which undergo reduction at low temperatures to Fe_3O_4 (15). The subsequent

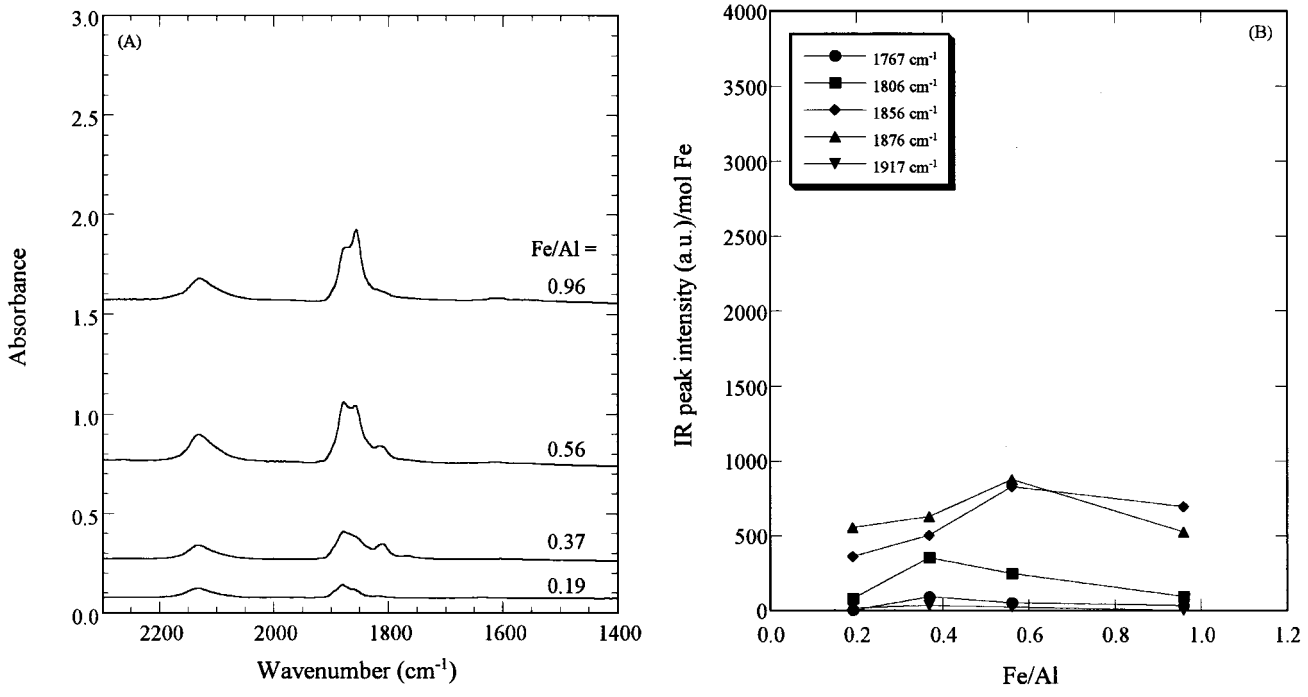

FIG. 10. (A) Infrared spectra of adsorbed NO for Fe–ZSM-5 samples following an oxidative pretreatment (O). (B) Intensity of infrared bands observed during the room-temperature adsorption of NO following an oxidative pretreatment (O) versus Fe content.

reduction of such particles from Fe_3O_4 to Fe^0 may occur at temperatures higher than those observed for bulk Fe_2O_3 because of the greater difficulty in reducing very small particles of Fe_3O_4 to Fe^0 (15).

The valence state of iron in Fe–ZSM-5 changes with the Fe/Al ratio. For Fe–ZSM-5-25 (0.14 and 0.19) the H_2/Fe consumption ratio determined from TPR experiments (see Table 3) is 1.34. This value is close to 1.5, the H_2/Fe

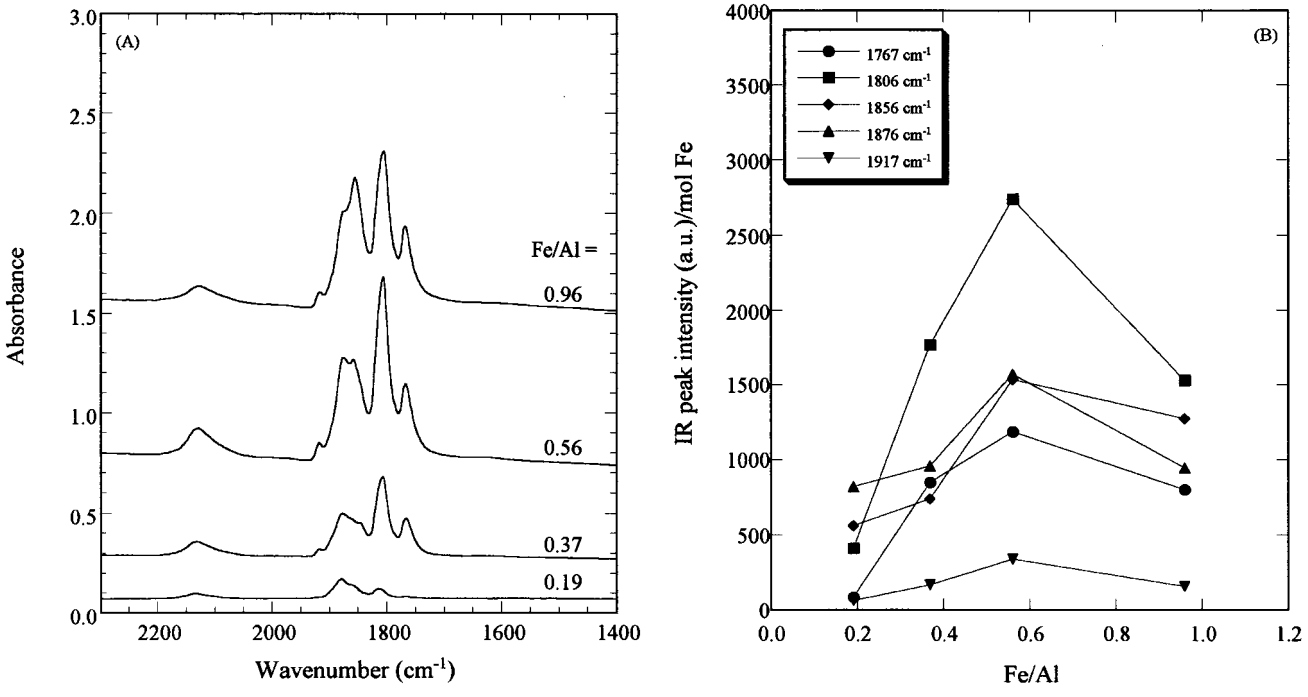

FIG. 11. (A) Infrared spectra of adsorbed NO for Fe–ZSM-5 samples following a reductive pretreatment (R). (B) Intensity of infrared bands observed during the room-temperature adsorption of NO following a reductive pretreatment (R) versus Fe content.

consumption ratio for reduction of Fe^{3+} to Fe^0, suggesting that, at low Fe/Al ratios, most of the Fe is present as Fe^{3+}. As discussed below, this conclusion is consistent with the observed low values of NO/Fe. It is also observed that oxidation of these samples does not increase the H_2/Fe consumption ratio significantly. The decrease in the H_2/Fe consumption ratio for He-pretreated Fe–ZSM-5-25 (0.37 and 0.56) and the increase in the consumption ratio upon oxidation of these samples suggests that the iron in the He-pretreated samples is present as a mixture of Fe^{3+} and Fe^{2+}. Comparison of the TPR spectra of these samples with those for samples for which Fe/Al = 0.14 and 0.19 suggests that, at higher Fe loadings, some of the Fe^{3+} is present in sites that allow Fe^{3+} to be reduced to Fe^0, whereas the balance is in sites that are only reducible to Fe^{2+}. Since Fig. 3 shows that, up to Fe/Al = 0.56, there continues to be a substitution of one Fe cation per Brønsted acid proton, it is concluded that all of the iron is dispersed cationically. Above a loading of Fe/Al = 0.56, small particles of Fe_2O_3 are formed. The rise in the H_2/Fe consumption ratio may be attributable to the reducibility of Fe_2O_3 to Fe^0. Comparison of the TPR spectra for Fe–ZSM-5 samples with Fe/Al = 0.85 and 0.96 with that for Fe/Al = 0.56 suggests that roughly half of the Fe in the highly loaded samples is dispersed as isolated Fe cations and the balance as small particles of Fe_2O_3.

An important issue to address is the pathway by which exchanged Fe^{3+} cations are reduced to Fe^{2+} during He pretreatment. If it is assumed that Fe enters the zeolite channels during the exchange as $FeCl_3$, the exchange process can be written as (3)

$$FeCl_3 + H^+Z^- \rightarrow [FeCl_2]^+Z^- + HCl_{(g)}. \qquad [1]$$

Following the initial ion exchange, the zeolite is washed in water. UV–visible spectra taken after exchange show bands at 244 and 346 nm due to iron chloride species. The disappearance of these bands after water washing is attributable to the removal of chlorine from the sample.

Since ferric ions have a strong tendency to hydrolyze (24), the following process can be envisioned:

$$[FeCl_2]^+Z^- + 2H_2O \rightarrow [Fe(OH)_2]^+Z^- + 2HCl. \qquad [2]$$

Elemental analysis showed that water washing did not result in a change in the amount of Fe in ZSM-5, indicating that the Fe that is ion-exchanged into ZSM-5 is not back-exchanged by protons coming from the water.

Prior to dehydration, it is assumed that all of the Fe which is cationically dispersed is present as $[Fe(OH)_2]^+Z^-$. However, dehydration of the samples following Reaction [2] could result in the autoreduction of some fraction of the ferric cations according to the following reactions:

$$2[Fe(OH)_2]^+Z^- \rightarrow 2[Fe(OH)]^+Z^- + H_2O + \tfrac{1}{2}O_2 \qquad [3]$$

and

$$[Fe(OH)_2]^+Z^- \rightarrow [FeO]^+Z^- + H_2O. \qquad [4]$$

Garten and co-workers proposed the conversion of Fe^{3+} to Fe^{2+} via a reaction similar to Reaction [3]. In their Mössbauer study on Fe–Y, it was observed that Fe^{2+} was formed as oxygen desorbed from the Fe^{3+} ions in hydrolyzed Fe–Y during evacuation at high temperature (24). Reaction [4] has not been demonstrated to occur, but is known for the autoreduction of Cu^{2+} to Cu^+ (25) (note that the charges on the atoms in Reaction [4] are as $[Fe^{2+}O^-]$).

Wichterlová and co-workers (26) have conducted experiments aimed at identifying the cation-exchange sites in ZSM-5. Using diffuse reflectance UV–vis and near-IR spectroscopy to characterize Co- and Cu-exchanged ZSM-5, ferrierite and mordenite, they determined that there are three types of sites present in these materials, designated as α, β, and γ. Figure 12 shows the locations of these sites in the ZSM-5 framework. The authors note that when both Co or Cu ions are exchanged into ZSM-5, they fill γ sites first, then β sites, and finally α sites as the M/Al ratio is increased. It was also shown for Cu–ZSM-5 that the Cu^{2+} present in α sites is most easily reduced, while that in the γ sites is most difficult to reduce. By analogy with these results, we suggest that, for Fe–ZSM-5-25 samples with an Fe/Al ratio ≤ 0.56, Fe fills primarily γ and β sites for samples with a very low loading of Fe [e.g., Fe–ZSM-5-25 (0.14 and 0.19)] and then as the Fe content increases the fraction of Fe occupying α sites increases. Above an Fe/Al ratio of 0.56 the Fe does not occupy α, β, or γ sites, but simply forms particles of FeO_x. Note also that the Fe which is present in the α sites on Fe–ZSM-5 (0.37 and 0.56) is easily reduced in He from Fe^{3+} to Fe^{2+} via autoreduction. However, the Fe^{2+} which is formed in this case may be difficult to reduce to Fe^0. Our results further suggest that Fe cations present in the γ and/or β sites do not easily autoreduce in He, but will reduce to Fe^0 in H_2.

The circumstances under which FeO_x particles are formed are not established by the present work. It is conceivable that during ion exchange small particles of $FeCl_3$ are nucleated within the pores of the zeolite when efforts are made to achieve a high level of exchange. Such nucleation may be triggered by Fe^{3+} cations already exchanged into the zeolites as $[FeCl_2]^+$ cations. Hydrolysis of these iron chloride clusters would lead to the formation of FeO_x particles. Alternatively, FeO_x particles might be formed by condensation of $[Fe(OH)_2]^+$ units during water washing of the as-exchanged zeolite. Yet, a third possibility is that FeO_x particles are formed during He pretreatment.

The results presented in Fig. 7 demonstrate that FeO_x particles can be reduced by CO. Iron carbonyls formed during this process may help disperse the Fe as Fe^{2+} cations since subsequent room-temperature exposure of Fe–ZSM-5-25 (0.96) to NO results in an enhanced NO adsorption capacity relative to that observed following He pretreatment (see Figs. 8 and 11).

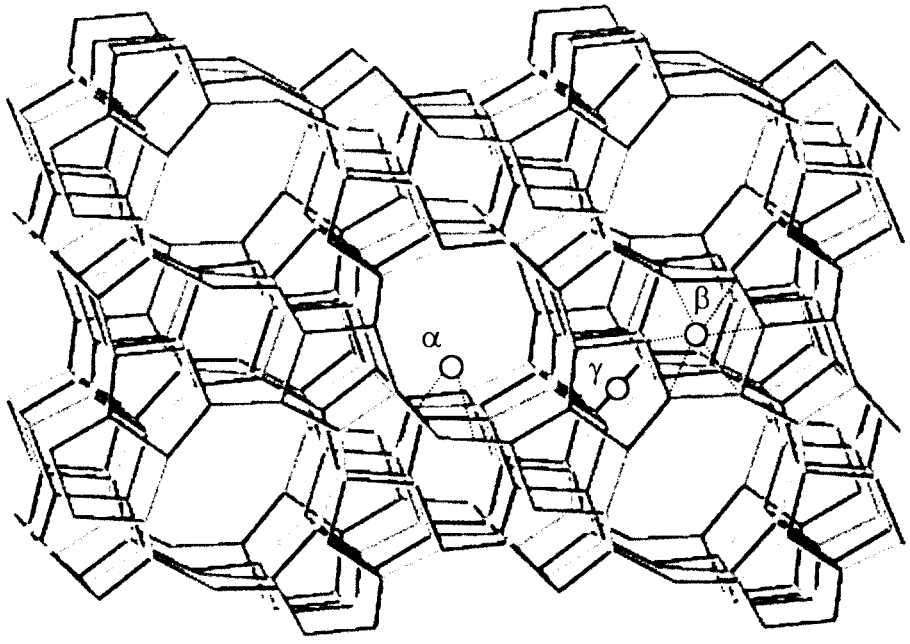

FIG. 12. Location of α, β, and γ sites in ZSM-5 (26). Note that lines indicate the location of the site and not the number of bonds of metal to the ZSM-5 framework.

The infrared spectra of adsorbed NO suggest that there are three types of Fe^{2+} species in Fe–H–ZSM-5. These can be defined as types I, II, and III sites. Type I sites are ascribed to Fe which adsorbs NO as both a mononitrosyl (at 1767 cm^{-1}) and a dinitrosyl (at 1917 and 1806 cm^{-1}). The bands at 1876 and 1856 cm^{-1} are due to mononitrosyls on Fe in two unique environments and are assigned to types II and III sites, respectively. Following He pretreatment, the NO adsorption observed at type I sites follows a pattern very similar to that observed during the NO uptake experiments (cf. Figs. 8B and 9B). It is observed that an increase in the Fe content up to an Fe/Al ratio of 0.56 results in an increase in the NO uptake based on both NO TPD and IR of adsorbed NO. Also, there is a significant decrease in the NO uptake for Fe–ZSM-5 (0.96) and the data in Fig. 9B show that the most significant loss in intensity occurs on Fe–ZSM-5 (0.96) for species present at type I sites. While there are changes in intensity with Fe content for Fe species at types II and III sites, the effect is not as dramatic as that observed for type I sites.

With the exception of Fe–ZSM-5-25 (0.19), oxidation clearly results in a decrease in the NO adsorption capacity for all samples, indicating that ferrous ions in Fe–ZSM-5 are oxidized in oxygen at 773 K (see Fig. 8). Types II and III sites exhibit a slight decrease in NO uptake following oxidation, but the most significant change in NO uptake relative to He pretreatment (H) occurs for type I sites (see Figs. 9B and 10B). Note also that the shape of the NO uptake curve is very similar to that observed for type I sites (most obvious for the band located at 1806 cm^{-1}).

The reduction of Fe^{3+} to Fe^{2+} by CO is demonstrated by NO uptake measurements and IR spectra of adsorbed NO (see Figs. 8 and 11B). As with oxidation, the effect of reduction on the Fe–ZSM-5 (0.19) sample is quite small. However, the adsorption capacities of all other Fe–ZSM-5 samples following a reductive pretreatment (R) increase dramatically, relative to that of samples following the oxidative treatment (O). Note that while all bands increase in intensity following CO reduction (relative to an oxidative pretreatment), there is a more dramatic increase for type I sites. These data, coupled with those observed previously, suggest that the Fe located at type I sites is readily oxidized and reduced relative to the Fe species located at the types II and III sites. Both the NO uptake measurements and IR data show that CO reduction results in what seems to be a redispersion of the Fe for Fe–ZSM-5 (0.96) relative to that with a He pretreatment. This is further confirmed by the H_2 TPR spectra shown in Fig. 7. The TPR pattern for Fe–ZSM-5 (0.96) following the reductive treatment shows the disappearance of the intense peak at 738 K, while the small peaks at higher temperatures exhibit only small changes. It is possible that the Fe species generating this peak is some form of FeO_x and that CO reduction results in a dispersion of this Fe to type I sites in the form of Fe^{2+}, thereby increasing the NO adsorption capacity and infrared band intensities. This is also confirmed by the H_2 uptake based on TPR in which the H_2/Fe consumption ratio following a CO reduction is 0.63, a value which is much smaller than that observed following a He or oxidative pretreatment on this sample. Note also that there is a significant increase in

the NO adsorption capacity (Fig. 8), suggesting that CO reduction results in both a redispersion of FeO_x species and a reduction of Fe^{3+} to Fe^{2+}.

The reduction of Fe–ZSM-5 by CO has little effect on the adsorption of NO or the intensities of the infrared bands for adsorbed NO with the exception of Fe–ZSM-5-25 (0.96) (see Figs. 8 and 11). As noted above, this sample shows a marked increase in the NO adsorption capacity relative to that observed following He pretreatment. Comparison of Figs. 9B and 11B shows that the most significant changes in the intensities of the infrared bands of adsorbed NO occurs for NO adsorbed on type I sites (1917, 1806, and 1767 cm^{-1}). What this indicates is that dispersion of the Fe in FeO_x upon CO reduction results in the placement of Fe atoms in type I sites. CO reduction appears to have little effect on the distribution of Fe in types II and III sites.

The pattern of change in Fe cations located in type I sites suggests that these are located in the α positions (see Fig. 12). Fe cations in this location are thought to be most readily reducible, and Wichterlová *et al.* (26) have shown that Cu cations in the α position form dinitrosyls, whereas Cu in β and γ positions form only mononitrosyls. On the basis of these considerations, we suggest that type I sites are located at the α position whereas types II and III sites are located at β and γ positions, although the exact correlations between these two methods of site designation cannot be defined.

CONCLUSIONS

The state of Fe in H–ZSM-5 as a function of Fe loading and pretreatment has been investigated. For samples with an Fe/Al ratio ≤ 0.56, Fe exchanges with Brønsted acid protons on a one-to-one basis, while higher weight loadings of Fe result in the formation of small particles of FeO_x. The oxidation state of Fe is a function of the Fe/Al ratio. For Fe/Al ≤ 0.19 most of the Fe is present as Fe^{3+} in the form of $[Fe(OH)_2]^+$, and at higher values of Fe/Al as a mixture of Fe^{3+} and Fe^{2+}. No adsorption occurs on Fe^{2+} cations and the NO/Fe uptake ratio correlates with the proportion of Fe present as Fe^{2+}. Three types of NO adsorption sites are identified, designated as I, II, and II. Type I sites adsorb NO as both mono- and dinitrosyls and are believed to be located on the walls of the straight and sinusoidal channels—the α positions shown in Fig. 12. Types II and III sites adsorb NO only as mononitrosyls and are located in the five- and six-membered rings—the β and γ positions shown in Fig. 12. CO reduction has little effect on the uptake of NO or the infrared spectrum of adsorbed NO for Fe/Al ≤ 0.56, but for Fe/Al $= 0.96$, CO reduction leads to a dispersion of the Fe in FeO_x particles into type I sites and a consequent rise in the uptake of NO.

ACKNOWLEDGMENTS

This work was supported by a grant from the National Science Foundation and, in part, by the Director of the Office of Basic Energy Sciences, Chemical Sciences Division, of the U.S. Department of Energy under Contract DE-AC03-76SF00098.

REFERENCES

1. Feng, X., and Hall, W. K., *Catal. Lett.* **41**, 45 (1996).
2. Feng, X., and Hall, W. K., *J. Catal.* **166**, 368 (1997).
3. Chen, H.-Y., and Sachtler, W. M. H., *Catal. Lett.* **50**, 125 (1998).
4. Chen, H.-Y., and Sachtler, W. M. H., *Catal. Today* **42**, 73 (1998).
5. Joyner, R. W., and Stockenhuber, M., *Catal. Lett.* **45**, 15 (1997).
6. Joly, J. F., Zanier-Szyldowski, N., Colin, S., Raatz, F., Saussey, J., and Lavalley, J. C., *Catal. Today* **9**, 31 (1991).
7. Hunger, B., Hoffmann, J., Heitzsch, O., and Hunger, M., *J. Therm. Anal.* **36**, 1379 (1990).
8. Topsøel, N.-Y., Pedersen, K., and Derouane, E. G., *J. Catal.* **70**, 41 (1981).
9. Schnabel, K.-H., Peuker, Ch., Parlitz, B., Löffler, E., Kürschner, U., and Kriegsmann, H., *Z. Phys. Chem.* **268**, 225 (1987).
10. Jacobs, P. A., and Von Ballmoos, R., *J. Phys. Chem.* **86**, 3050 (1982).
11. Bordiga, S., Platero, E. E., Arean, C. O., Lamberti, C., and Zecchina, A., *J. Catal.* **137**, 179 (1992).
12. Kustov, L. M., Kazansky, V. B., Beran, S., Kubelkova, L., and Jiru, P., *J. Phys. Chem.* **91**, 5247 (1987).
13. Quin, G., Zheng, L., Xie, Y., and Wu, C., *J. Catal.* **95**, 609 (1985).
14. Munteanu, G., Ilieva, L., and Andreeva, D., *Therm. Acta* **291**, 171 (1997).
15. Yuen, S., Chen, Y., Kubsh, J. E., Dumesic, J. A., Topsøe, N., and Topsøe, H., *J. Phys. Chem.* **86**, 3022 (1982).
16. Contour, J. P., and Mouvier, G., *J. Catal.* **40**, 342 (1975).
17. Segawa, K., Chen, Y., Kubsh, J. E., Delgass, W. N., Dumesic, J. A., and Hall, W. K., *J. Catal.* **76**, 112 (1982).
18. Aparico, L. M., Hall, W. K., Fang, S., Ulla, M. A., Millman, W. S., and Dumesic, J. A., *J. Catal.* **108**, 233 (1987).
19. Iwamoto, M., Yahiro, H., Mizuno, N., Zhang, W.-X., Mine, Y., Furukawa, H., and Kagawa, S., *J. Phys. Chem.* **96**, 9360 (1992).
20. Giamello, E., Murphy, D., Magnacca, G., Morterra, C., Shioya, Y., Nomura, T., and Anpo, M., *J. Catal.* **136**, 510 (1992).
21. Valyon, J., and Hall, W. K., *J. Phys. Chem.* **97**, 1204 (1993).
22. Hoost, T. E., Laframboise, K. A., and Otto, K., *Catal. Lett.* **33**, 1105 (1995).
23. Hadjiivanov, K., Saussey, J., Freysz, J. L., and Lavalley, J. C., *Catal. Lett.* **52**, 103 (1998).
24. Garten, R. L., Delgass, W. N., and Boudart, M., *J. Catal.* **18**, 90 (1970).
25. Larsen, S. C., Aylor, A. W., Bell, A. T., and Reimer, J. A., *J. Phys. Chem.* **98**, 11533 (1994).
26. Wichterlová, B., Dedecek, J., and Sobalik, Z., *in* "Proceedings of the 12th International Zeolite Conference" (M. M. J. Treacy, B. K. Marcus, M. E. Bisher, and J. B. Higgins, Eds.), p. 941. Materials Research Society, Baltimore, MD, 1998.